Supporting Information

Quantified Hole Concentration in AlGaN Nanowires for High-Performance Ultraviolet Emitters

Chao Zhao,[a] Mohamed Ebaid,[a] Huafan Zhang,[a] Davide Priante,[a] Bilal Janjua,[a] Daliang Zhang,[b] Nini Wei,[b] Abdullah A. Alhamoud,[a] Mohammad Khaled Shakfa,[a] Tien Khee Ng,*[a] and Boon S. Ooi*[a]

[a] King Abdullah University of Science and Technology (KAUST), Photonics Laboratory, Thuwal 23955-6900, Saudi Arabia

[b] King Abdullah University of Science and Technology (KAUST), Imaging and Characterization Core Lab, Thuwal 23955-6900, Saudi Arabia

*Email: tienkhee.ng@kaust.edu.sa

*Email: boon.ooi@kaust.edu.sa

1. SEM images of AlGaN nanowires grown with different T_{Mg}

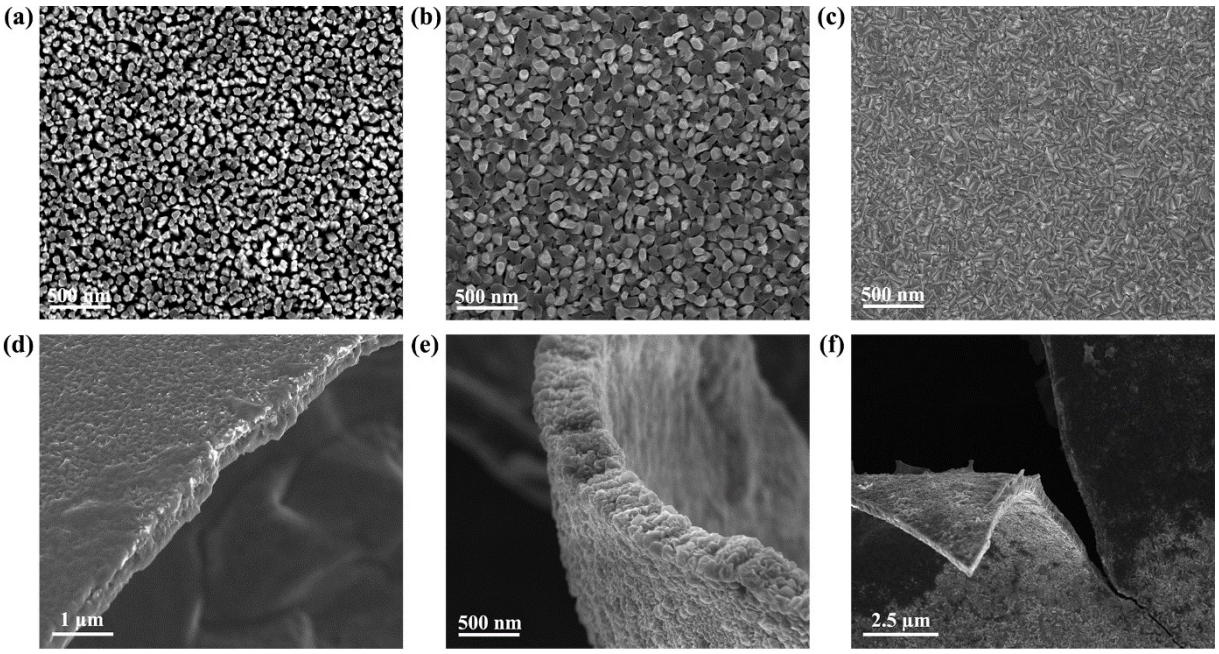

Fig. S1 Plan-view SEM images of AlGaN nanowires grown with (a) T_{Mg} = 320 °C, (b) T_{Mg} = 360 °C, (c) T_{Mg} = 440 °C. (d-f) SEM images of quasi-AlGaN layers from samples grown with T_{Mg} = 400 °C and T_{Mg} = 440 °C.

2. RT PL and Raman spectra of AlGaN nanowires grown with different T_{Mg}

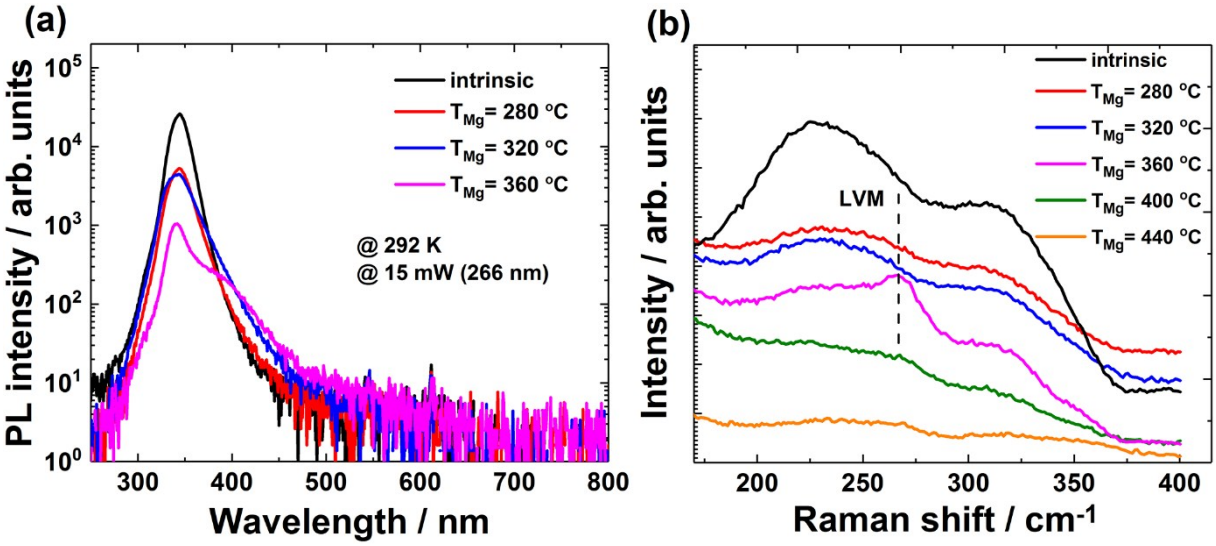

Fig. S2 (a) RT PL and (b) Raman spectra of the AlGaN nanowires grown with different T_{Mg}.

3. OCP measurements of all the samples

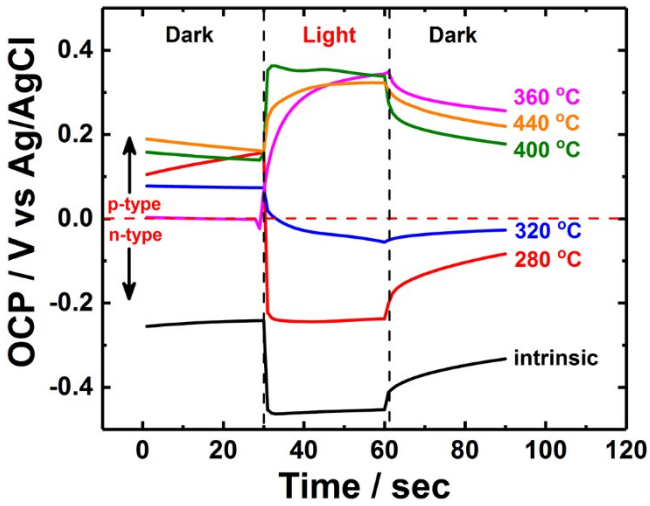

Fig. S3 OCP of AlGaN nanowires as a function of T_{Mg}.

The OCP of all AlGaN nanowire samples was measured as a function of T_{Mg} in a three-electrode PEC cell under dark and illumination conditions. With increasing T_{Mg}, the OCP shift was changed from negative to positive indicating a systematic transition from n- to p-type conductivity. The AlGaN-nanowire samples doped with a T_{Mg} equal to or higher than 360 °C exhibited a p-type conductivity.

4. Mott-Schottky analysis of p-type Si

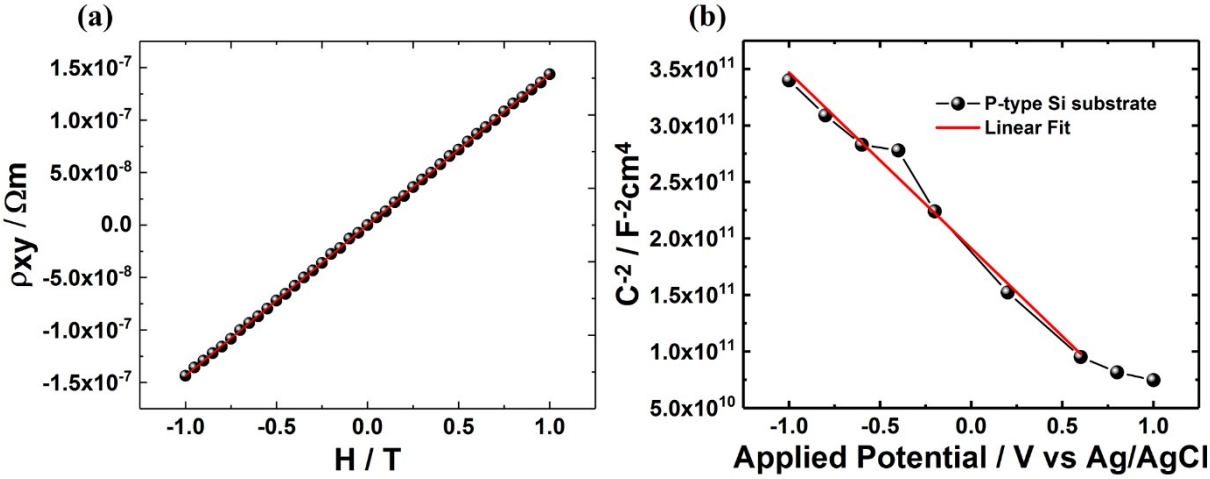

Fig. S4 (a) Magnetic field dependence of the Hall resistivity measured at RT. (b) Mott-Schottky plot of the bare p-type Si substrate.

A p-type Si substrate was used as a reference to verify the evaluation process by comparing results from Hall measurement and Mott-Schottky. The Four point probe measurement showed

a resistivity of 0.004 Ω·cm, which is in the range with the resistivity level specified by the vendor (0.001-0.005 Ω·cm). The carrier concentration measured from magnetic field dependence of the Hall resistivity in Hall measurement was 4.35×10^{19} cm^{-3}, as shown in Fig. S4(a). We also extracted a carrier concentration of 5.82×10^{19} cm^{-3} from a linear fitting of the Mott-Schottky plot, as shown in Fig. S4b.

5. Mott-Schottky analysis of AlGaN nanowires

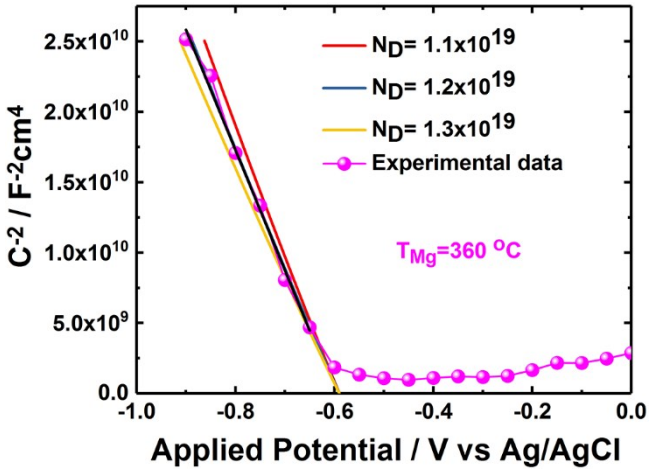

Fig. S5 Fitting of Mott-Schottky curves of the representative AlGaN-nanowire sample doped with T_{Mg} of 360 °C with the new equations solved in the cylindrical coordinates.

The solid lines in the above figure refer to the fitting data of the experimental Mott-Schottky plots. Each of the fitting lines gives a net ionized dopant density value. The approximated value of the net ionized dopant density can be then selected from the line that is well matching with the experimental data. The net ionized dopant density of the sample doped with a T_{Mg} of 360 °C was 1.3×10^{19} cm^{-3},[1] which is a high hole carrier density due to the enhanced Mg incorporation at low growth temperature and small activation energy of Mg in nanowires.[2]

6. FIB samples preparation and STEM images of nanowires

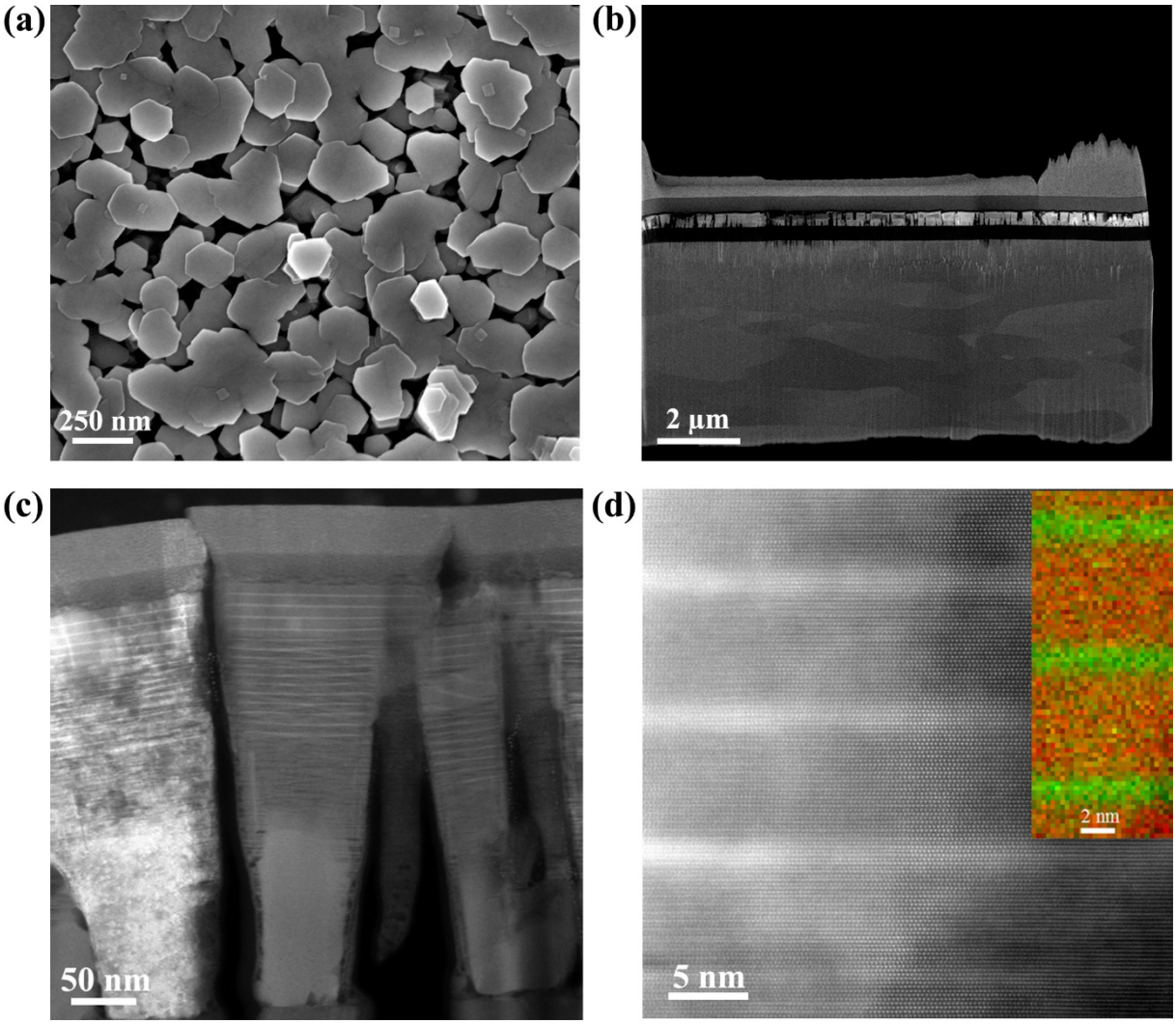

Fig. S6 (a) Plan-view SEM image of FIB region with nanowire UV LEDs. (b) SEM image of the FIB lamella. HAADF-STEM images of (c) nanowire UV LEDs and (d) AlGaN/AlGaN Qdisks, the inset shows a combined false-color elemental concentration maps of Qdisks with Ga in green and Al in red.

7. NEXTNANO simulation

One-dimensional modeling was performed to understand the carrier dynamics in the quantum-confined structures using the commercially available NEXTNANO[3] software under a forward bias. The nitrogen polarity was assumed in the simulation, which is an important parameter in determining the direction of the polarization fields. The emission wavelength of the Qdisks was 335 nm with 14 % Al. Fig. S7(a) shows the calculated band diagram for the Qdisks-based nanowire UV LED under a forward bias of 4 V, which was obtained by self-

consistently solving Poisson's, Schrodinger's, current continuity, and carrier transport equations. We considered the effects of wavefunction overlap in the $Al_{0.14}Ga_{0.86}N$ (1.6 nm)/$Al_{0.3}Ga_{0.7}N$ (6 nm)-based active region and the polarization induced band bending due to the interface fixed charges. One dimensional (1D) strain was imported from the center of the realized 3D nanowire model based on strain energy minimization algorithm. Thus, the reduced volume-related strain reduction in nanowires was considered. Hole doping density of 1.3×10^{19} cm^{-3}, as estimated by the Mott-Schottky measurement, was utilized in solving the current problem. Fig. S7(b) shows a large electron-hole wavefunction overlap of 38.7 % because of the reduced strain and thinner $Al_{0.14}Ga_{.86}N$ Qdisks, as shown in Fig. S7(c). The calculated recombination rates in the active region show that direct radiative recombination is the dominant form of recombination (see Fig. S7(d)). In the presence of a large number of wells, the average carrier density is considerably reduced, which suppresses the Auger recombination. A decrease in the barrier height is expected at the n-$Al_{0.3}Ga_{0.7}N$/GaN interfaces by incorporating an intermediate composition, thin $Al_{0.15}Ga0_{.85}N$ layer (5 nm) compared to the conventional abrupt interface, and the decrease in the barrier height can significantly enhance the carrier injection efficiency of our device.[3]

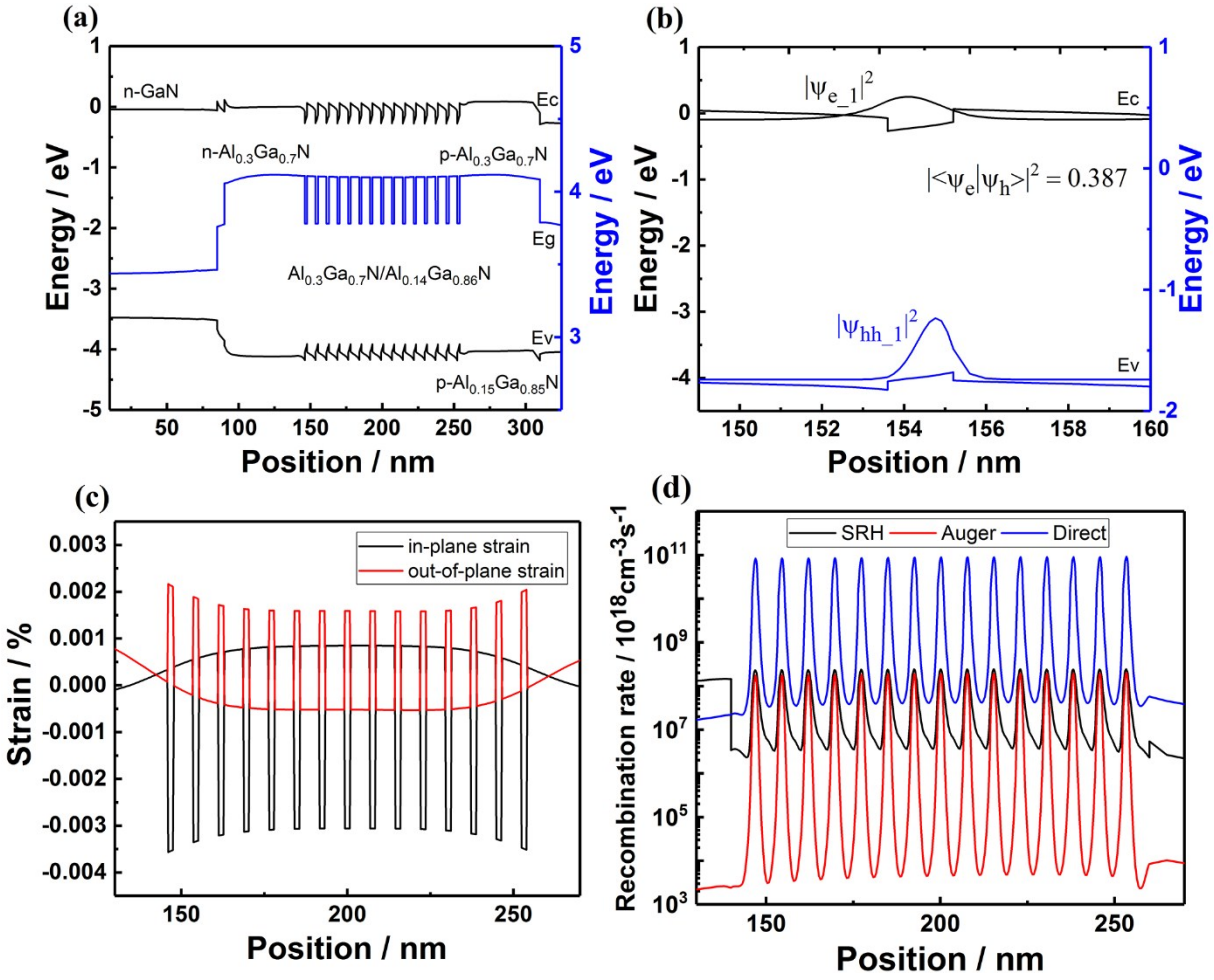

Fig. S7 (a) The band profile of the $Al_{0.14}Ga_{.86}N$/ $Al_{0.3}Ga_{0.7}N$ Qdisk under a forward bias of 4 V. (b) Wave function profiles corresponding to the electrons and holes in the active region. (c) Strain distribution. (d) Recombination rates including Shockley-Read-Hall (SRH), Auger, and direct recombination in the active region.

8. Raman spectra of the UV LED under different biases

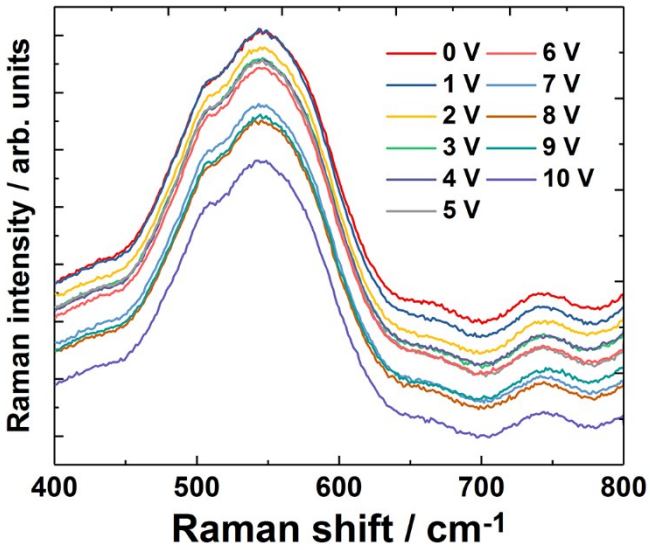

Fig. S8 Raman spectra of the UV LED under different biases.

REFERENCES

1. Cimpoiasu, E.; Stern, E.; Klie, R.; Munden, R. A.; Cheng, G.; Reed, M. A. *Nanotechnology* **2006**, *17*, 5735.

2. Mi, Z.; Zhao, S.; Woo, S. Y.; Bugnet, M.; Djavid, M.; Liu, X.; Kang, J.; Kong, X.; Ji, W.; Guo, H.; Liu, Z.; Botton, G. A. *J. Phys. D: Appl. Phys.* **2016**, *49*, 364006.

3. Lähnemann, J.; Den Hertog, M.; Hille, P.; de la Mata, M. a.; Fournier, T.; Schörmann, J.; Arbiol, J.; Eickhoff, M.; Monroy, E. *Nano Lett.* **2016**, *16*, 3260-3267.